

# A TIME DOMAIN MOMENT TENSOR INVERSION TECHNIQUE AND ITS VERIFICATION

J.-Y. CHING AND S. D. GLASER

University of California at Berkeley  
485 Davis Hall, University of California, Berkeley, CA 94710, USA

## ABSTRACT

A time domain moment inversion method has been developed for identification of internal damage mechanisms in rock. This method makes use of full waveforms, instead of first arrivals, of signals received by NBS-type high-fidelity sensors to invert the damage mechanisms. The flat frequency response of NBS-type sensors enables us to yield signals comparable to mathematical solutions. This makes it possible to study the damage mechanism mathematically using the moment tensor inversion. Our current work includes conducting experiments on a Gypsum cube. Artificial acoustic sources made by piezoelectric elements are cast in the cube and used to simulate rock damages. By inverting the simulating signals, we could verify the validity of the time domain moment tensor inversion scheme.

## INTRODUCTION

The goal of our research is to characterize damage mechanisms inside of rock structures, using an approach based on fundamental physical principles. The best technique available to map the internal kinematics of the smallest dislocations is microseismic (acoustic emission, AE) monitoring of the elastic waves generated in conjunction with internal deformations. Optimal extraction of information from the microseismic signal requires the use of very high-fidelity sensors so that a sizable length of source-dependent time history can be used to evaluate the internal dislocation. This paper presents preliminary results from the application of a full-waveform time-domain inversion process to such high fidelity signals to map internal crack kinematics.

The technique we employ for inverting the dislocation kinematics is time domain moment tensor inversion [1]. Moment tensor inversion is a common method used by geophysicists to describe the mechanics of a seismic point source [2] [3]. It has also been applied to AE signals [4], sometimes with very good results [5]. Proper application of any inversion scheme, however, requires unambiguous identification of wave mode arrival, which cannot be made with the conventional transducers and monitoring systems used. We avoid this difficulty by employing our high-fidelity sensors. It has been demonstrated that careful use of this type of high fidelity device yields waveforms strictly proportional to the actual source kinematics, although affected by travel through the host material [6] [7] [8] [9]. The quality of the signals recorded allows direct interpretation of source mechanisms from wave propagation theory.

The purpose of this paper is to verify the inversion scheme by presenting results of experiments performed with known sources and a well-characterized medium. A conical piezoelectric element was cast in a test block constructed from a very uniform rock-like material to serve as acoustic sources. In each experiment, the element is activated by a repeatable driving signal to generate transient acoustic waves. Each experiment consists the same source but different sensor locations, and the moment tensor of the source is then estimated for each experiment. The verification of the inversion scheme is made by comparison of the identified moment tensors: If the inverted moment tensors from different experiments are qualitatively similar, we conclude the inversion scheme converges to a valid result.

## THEORY OF THE MOMENT TENSOR

Assume an elastic solid with external boundary  $\mathbf{S}$  subjected to homogeneous external boundary conditions, and containing an internal (buried) boundary  $\Sigma$ . If the body force on the elastic solid is ignored, the external displacement field can be represented as a function of a dislocation on  $\Sigma$  as follows [2] [3] [9]:

$$u_n(x, t) = \int_{\Sigma} \langle u_i(\xi, t) \rangle \cdot C_{ijpq} \cdot v_j \otimes G_{np,q}(x, t; \xi, 0) \cdot d\xi \quad (1)$$

where  $\otimes$  is the convolution operator,  $\langle u_i(\xi, t) \rangle$  is the dislocation time history at  $\xi$  ( $\xi \in \Sigma$ ),  $u_n(\mathbf{x}, t)$  is the time history of the  $n$ -th component displacement at  $\mathbf{x}$ ,  $C_{ijpq}$  is the elastic constitutive tensor,  $v_j$  the vector normal to  $\Sigma$ ,  $G_{np}$  is the elasto-dynamic Green's function and  $G_{np,q}$  denotes  $\partial G_{np} / \partial \xi_q$ .

If the observed wave lengths are much larger than the source size, we can approximate the source as a point source, avoid integration over  $\Sigma$ , and write [10]

$$u_n(x, t) = M_{pq}(t) \otimes G_{np,q}(x, t; \xi, 0) \quad \text{where } M_{pq}(t) = \int_{\Sigma} \langle u_i(\xi, t) \rangle \cdot C_{ijpq} v_j d\xi. \quad (2)$$

Letting  $\mathbf{x}$  in Eqn. 2 be the location of a AE sensor,  $u_n(\mathbf{x}, t)$  represents the history of the measured displacements normal to the sensor mounting surface, since the AE sensors used for this study can only detect normal displacement. For each sensor, say the  $j$ -th sensor, the following equation holds-

$$u^j(t) = M_{pq}(t) \otimes \Gamma_{pq}^j(t) \quad (3)$$

where  $u^j(t)$  is the measured displacement history by sensor  $j$ ,  $\mathbf{n}$  is the direction normal to the mounting surface, and  $\Gamma_{pq}^j(t)$  is the same as  $G_{np,q}(\mathbf{x}^j, t; \xi, 0)$  since  $\mathbf{x}^j$  is the location of the  $j$ -th sensor and.

Equation 3 can be transformed from a continuous to a discrete time equation:

$$u^j(k) = M_{pq}(k) \otimes \Gamma_{pq}^j(k) \quad (4)$$

where  $\otimes$  is now discrete-time convolution, and  $\mathbf{k}$  is the time-step. Equation 4 in matrix form becomes

$$\underline{U}^j = \underline{\Gamma}^j \cdot \underline{M} \quad (5)$$

where

$$\underline{U}^j = [u^j(0) \quad u^j(1) \quad \dots \quad u^j(n)]^T \quad (6)$$

$$\underline{M} = [M_{11}(0) \quad M_{11}(1) \quad \dots \quad M_{11}(n) \quad M_{22}(0) \quad M_{22}(1) \quad \dots \quad M_{13}(n-1) \quad M_{13}(n)]^T \quad (7)$$

$$\underline{\Gamma}^j = [\underline{\Gamma}_{11}^j \quad \underline{\Gamma}_{22}^j \quad \underline{\Gamma}_{33}^j \quad \underline{\Gamma}_{12}^j \quad \underline{\Gamma}_{23}^j \quad \underline{\Gamma}_{13}^j] \quad (8)$$

$$\underline{\Gamma}_{pq}^j = \alpha \cdot \begin{bmatrix} \Gamma_{pq}^j(0) & 0 & 0 & \dots & 0 \\ \Gamma_{pq}^j(1) & \Gamma_{pq}^j(0) & 0 & \dots & 0 \\ \Gamma_{pq}^j(2) & \Gamma_{pq}^j(1) & \Gamma_{pq}^j(0) & \dots & \vdots \\ \vdots & \vdots & \vdots & \ddots & \vdots \\ \Gamma_{pq}^j(n) & \Gamma_{pq}^j(n-1) & \Gamma_{pq}^j(n-2) & \dots & \Gamma_{pq}^j(0) \end{bmatrix} \quad (9)$$

where  $\alpha = 1$  if  $\mathbf{p}=\mathbf{q}$ , 2 if  $\mathbf{p} \neq \mathbf{q}$ .

Suppose there are  $\mathbf{N}$  acoustic sensors mounted at different locations, we would have  $\mathbf{N}$  matrix equations like Eqn. 5. Combining the  $\mathbf{N}$  matrix equations into one, we get

$$\underline{U} = \underline{\Gamma} \cdot \underline{M} \quad (10)$$

where

$$\underline{U} = [u^1(0) \quad u^1(1) \quad \cdots \quad u^1(n) \quad u^2(0) \quad \cdots \quad u^2(n) \quad \cdots \quad \cdots \quad u^N(n-1) \quad u^N(n)]^T \quad (11)$$

$$\underline{\Gamma} = \begin{bmatrix} \underline{\Gamma}_{11}^1 & \underline{\Gamma}_{22}^1 & \underline{\Gamma}_{33}^1 & \underline{\Gamma}_{12}^1 & \underline{\Gamma}_{23}^1 & \underline{\Gamma}_{13}^1 \\ \underline{\Gamma}_{11}^2 & \underline{\Gamma}_{22}^2 & \underline{\Gamma}_{33}^2 & \underline{\Gamma}_{12}^2 & \underline{\Gamma}_{23}^2 & \underline{\Gamma}_{13}^2 \\ \underline{\Gamma}_{11}^3 & \underline{\Gamma}_{22}^3 & \underline{\Gamma}_{33}^3 & \underline{\Gamma}_{12}^3 & \underline{\Gamma}_{23}^3 & \underline{\Gamma}_{13}^3 \\ \vdots & \vdots & \vdots & \vdots & \vdots & \vdots \\ \vdots & \vdots & \vdots & \vdots & \vdots & \vdots \\ \underline{\Gamma}_{11}^N & \underline{\Gamma}_{22}^N & \underline{\Gamma}_{33}^N & \underline{\Gamma}_{12}^N & \underline{\Gamma}_{23}^N & \underline{\Gamma}_{13}^N \end{bmatrix} \quad (12)$$

Equation 10 is most convenient for solving forward problems (one knows  $\underline{\Gamma}$  and  $\underline{M}$  and would like to calculate  $\underline{U}$ ). For the inverse problem (moment tensor inversion), one knows  $\underline{\Gamma}$  and  $\underline{U}$  but would like to estimate  $\underline{M}$ . From examination of Eqn. 10, it is seen that the inversion for  $\underline{M}$  is simply a least square problem [11].

The inversion utilizes full waveforms to invert source functions. This can be easily seen from Eqn. 10~12: the  $\underline{U}$  vector used to invert source functions contains  $n$  sampling points of the received signals. Compared to the inversion methods using only first arrivals, our inversion scheme extracts more information from the signal data. We are able to achieve this because we use the high-fidelity NBS-type sensors, which yield waveforms strictly proportional to the actual displacement time histories. By taking full waveforms, we are able to invert for the “evolution” rather than the first motion of the source processes.

The premise for utilizing full waveform is the availability of the correct Green’s functions, that is, the  $\underline{\Gamma}$  matrix in Eqn. 10. For identifying sources in a half space, the analytical solutions of Lamb’s problem [12] will be the Green’s functions. For sources in an elastic solid with complicated geometry, analytical solutions are often unavailable. Numerical solutions (e.g. boundary element, finite element, etc.) of an elasto-dynamic problem with appropriate boundary conditions can be employed as Green’s functions.

### EXPERIMENT STUDY

Some experiments have been conducted in laboratory. The purpose of the experiments is to validate the appropriateness of the inversion scheme. The experiments are carried out on a 300 mm cube of Die-Keen, a gypsum cement used for making dental molds which results in a very homogeneous body due to low (<0.20%) expansion during hydration [13]. Die-Keen has a density of 2.3 g/cc, a dry compressive strength of 2.2 MPa, a P-wave velocity of 3.50 mm/ $\mu$ s and a S-wave velocity of 2.08 mm/ $\mu$ s, both measured at 250 kHz [14]. Several different piezoelectric elements were cast in the block with thin electrical leads exiting the block to allow the elements to act as artificial acoustic sources. The element is driven by a computer-controlled arbitrary signal generator and gated amplifier [14]. As the element is excited, elastic waves are generated and propagate toward the external boundary, and measured by the acoustic sensors. Based on “triangulation” of P-wave arrival time differences at the various sensors, the pseudo-point source is located and the appropriate Green’s functions are calculated. Equation 10 and  $QR$  decomposition are used to estimate  $\underline{M}$ . The estimated  $\underline{M}$  is denoted by  $\underline{M}^{\text{est}}$ .

The actual high voltage transient signal that activates the buried element has been found to be very repeatable. For independent trials, if the positions of the sensors are changed,  $\underline{M}^{\text{est}}$  should remain the same. This is the criterion used to validate the inversion scheme. The results from few experiments will be shown in this paper.

Glaser-type high-fidelity sensors, based on NBS design, are used for the experiments. These sensors are wide-banded sensors with relatively flat frequency response from 10 kHz to 1 MHz. The signals from the sensors, pre-conditioned by an internal FET-based circuit imparting 11 dB gain, are sent to the external amplifier (Fuji Ceramics model A1002), which has a nominal gain of 55 dB [15]. A Hi-Techniques 600 digitizer was used to extract the signals generated from the sensors. The digitizer provides data streaming directly to disk (10 Msamples/s per channel) and continuous waveform time-stamping up to plus/minus 50 ns. Triggering capabilities include four-channel full and/or logic modes with user configurable timed trigger windows, which reject trigger from events occurring outside of the predetermined fracture zone.

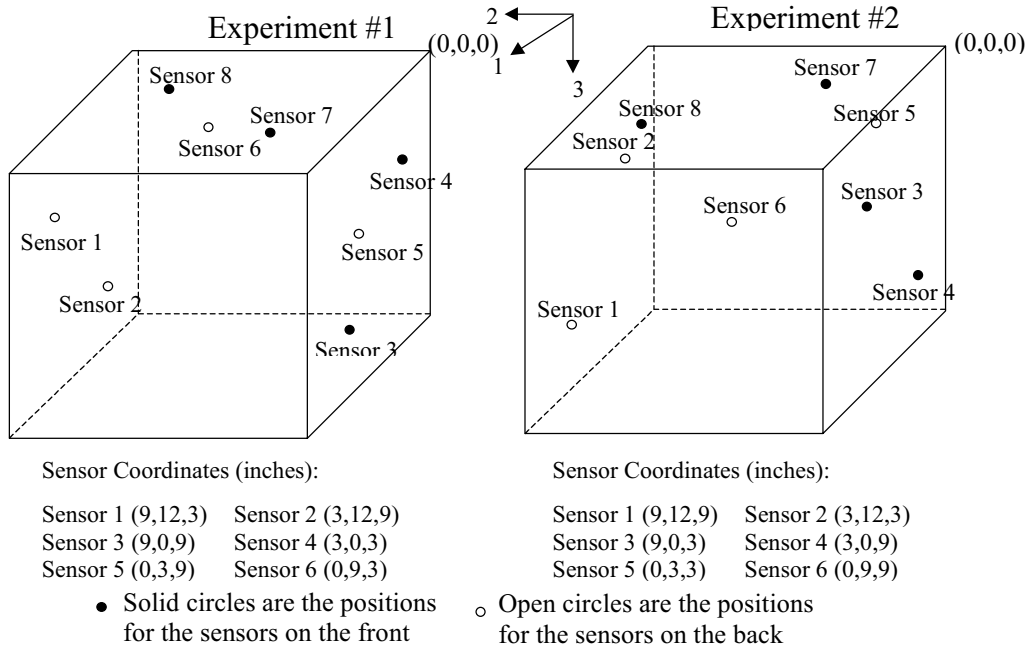


Figure 1 The relative positions of the sensors of the two experiments

We will only show the results of two experiments in this paper. The two experiments used the same conical piezoelectric element as the source, while the positions of the sensors were changed. The relative positions of the sensors of the two experiments are shown in Fig. 1. Since the signals were generated by the same source, we expect the identified moment tensors from these two experiments to be congruent. The detected displacement history from the sensors in the two experiments are shown in Fig. 2.

The first arrivals of P-wave energy were picked and used to locate the source for the two experiments. The calculated source positions for the two sets of data were within 5 mm. Given the source location, the Green's functions can be calculated. In this paper, we use half-space Green's functions as approximations to cube Green's functions. The main difference between the two is that the latter contains reflections from the sides of the cube. This approximation is good up to the arrival of the first reflection from the sides. This means that we need to truncate the sensor signals at the arrival time the first reflection. For the gypsum cube, the first reflection from the sides arrives approximately around S wave arrival time. So we actually only use the information of P wave to invert the source functions in this paper. To use information of S wave and R wave requires the Green's functions of a cube, which is the subject of our next paper. Fig. 3 shows the identified moment tensors from the two experiments.

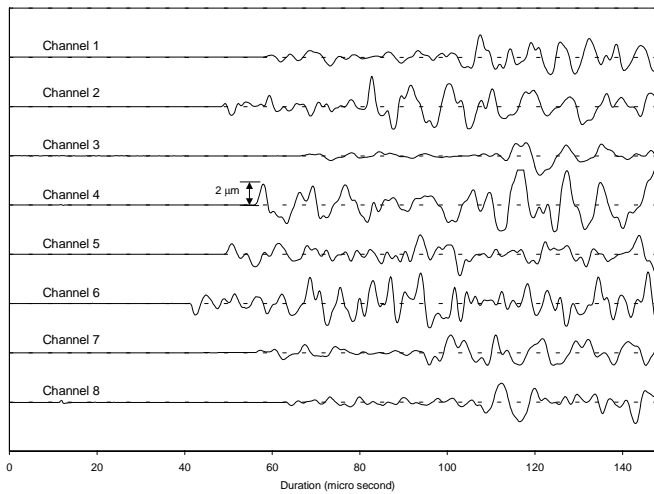
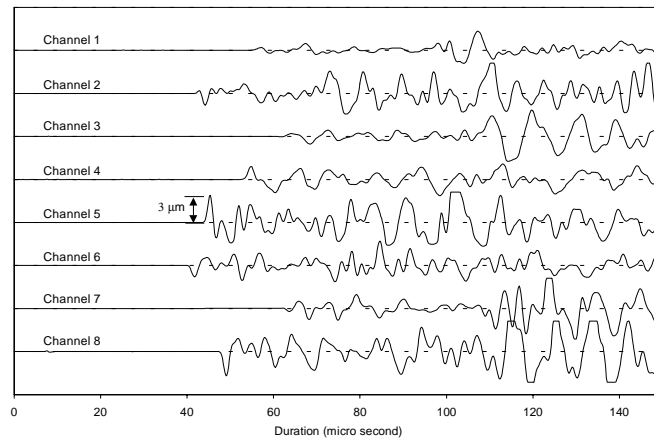


Figure 2 The detected displacement history from the sensors. (upper is for experiment #1 and lower is for experiment #2)

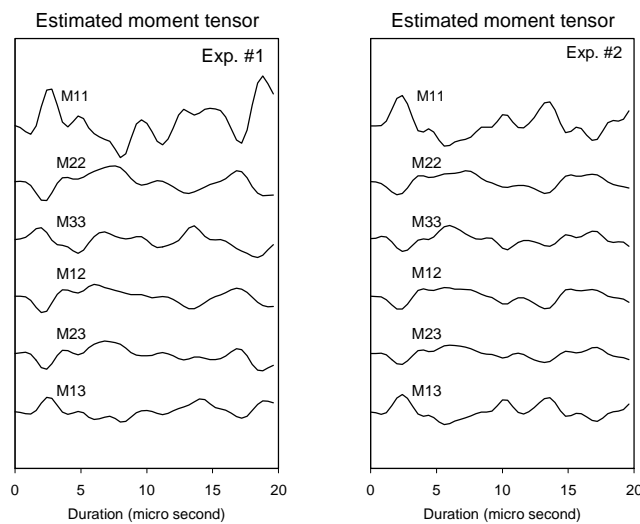


Figure 3 The identified moment tensors from the two experiments

It is clearly seen that, in spite of the fact that the sensor locations are changed for the two experiments, the estimated moment tensors are quite similar. We hope, by conducting more experiments with the same source but different sensor locations, the similarity can still exist. Then we can conclude that our inversion scheme is reliable.

## CONCLUSIONS

The time-domain approach for moment tensor inversion has been introduced. This approach characterizes with a linear estimation scheme of least square method. Two experiments with the same artificial source but different sensor locations are conducted. The results of the two experiments indicate that the estimates of the source function are similar. This implies the time domain inversion scheme is valid.

## ACKNOWLEDGEMENTS

This research has been supported by National Science Foundation Grant # CMS-9727002. Special thanks to Professor Lane Johnson for his guidance and tutelage.

## REFERENCES

1. Michaels, J.E., Michaels, T.E, and Sachse, W. (1981), Applications of Deconvolution to Acoustic Emission Signal Analysis, *Materials Evaluation*, 39(10), pp. 1032-1036.
2. Jost, M.L. and R.B. Herrmann (1989). A student's guide to and review of moment tensors. *Seismological Research Letters*, 60, 2, 37-57.
3. Aki, K. and P.G. Richards (1980). *Quantitative Seismology*. Freeman, San Francisco.
4. Ohtsu, M. (1991). Simplified moment tensor analysis and unified decomposition of acoustic emission source: application to in situ hydrofracture test. *Journal of Geophysical Research*, 1B, 6211-6221.
5. Shah, K.R. and J.F. Labuz (1995). Damage mechanisms in stressed rock from acoustic emission. *Journal of Geophysical Research*, 100, B8,15527-15539.
6. Glaser, S.D., G. Weiss, and L.R. Johnson (1998). Body waves recorded inside an elastic half space by an embedded, wideband velocity sensor. *Journal of the Acoustical Society of America*, 104(3), 1404-1412.
7. Greenspan, M. (1987). The NBS Conical Transducer: Analysis. *Journal of the Acoustical Society of America*, 81(1), pp 173-183.
8. Proctor, T.M. Jr., (1986). More-Recent Improvements on the NBS Conical Transducer," *Journal of Acoustic Emission*, 5(4), pp. 134-142.
9. Eitzen, D. G., Breckenridge, F. R., Clough, R. B., Fuller, E. R., Hsu, N. N., and Simmons, J. A. (1981). Fundamental Developments for Quantitative Acoustic Emission Measurements, *Interim Report NP-2089*, prepared for Electric Power Research Institute.
10. Stump, B.W. and L.R. Johnson (1977). The determination of source properties by the linear inversion of seismograms. *Bulletin of Seismological Society of America*, 67, 6, 1489-1502.
11. Sorenson, H.W. (1970). Least-squares estimation from Gauss to Kalman. *IEEE Spectrum*, 7(7), pp. 63-68.
12. Johnson, L.R. (1974). Green's function for Lamb's problem, *Geophys. J. R. astr. Soc.*, 37, pp. 99-131.
13. Heraeus Kulzer, Inc. (1996). *Modern Materials: Dental Gypsum and Plaster Materials Material and Safety Data Sheet*. South Bend, IN: Heraeus Kulzer, Inc. Dental Products Division.
14. Glaser, S. D., and Hand, M. Y. (1998). Imaging of Rock Fractures with Low-Frequency Ultrasonic Reflection/Diffraction, *Geotechnical Testing Journal*, 21(4), pp. 317-327.
15. Weiss, G. and Glaser, S. D. (1998), Design and Absolute Calibration of an Embedded, Wideband Velocity Sensor, *Transportation Research Record* 1614, pp. 43-51.